

# Constraints On Dark Energy Models From Galaxy Clusters and Gravitational Lensing Data

Alexander Bonilla<sup>1,\*</sup> and Jairo E. Castillo<sup>2,†</sup>

<sup>1</sup>*Departamento de Física, Universidade Federal de Juiz de Fora, 36036-330, Juiz de Fora, MG, Brazil*

<sup>2</sup>*Facultad Tecnológica, Unversidad Distrital Francisco José de Caldas, Carrera 7 No. 40B - 53, Bogotá, Colombia*

The Sunyaev-Zeldovich (SZ) effect is a global distortion of Cosmic Microwave Background (CMB) spectrum as result of its interaction with a hot electron plasma in the intracluster medium of large structures gravitationally viralized such as galaxy clusters (GC). Furthermore, this hot gas of electrons emits X-Rays due to its fall in the gravitational potential well of the GC. The analysis of SZ and X-Ray data, provide a method for calculating distances to GC at high redshifts. On the other hand, many galaxies and GC produce a Strong Gravitational Lens (SGL) effect, which has become a useful astrophysical tool for cosmology. We use these cosmological tests in addition to more traditional ones to constrain some alternative dark energy (DE) models, including the study the history of expansion through the cosmographic parameters. Using Akaike and Bayesian Information Criterion we find that the  $w$ CDM and  $\Lambda$ CDM models are the most favoured by the observational data. In addition, we found that at low redshift appears a peculiar behavior of slowdown, which occurs in some dynamical DE models using data only from GC.

PACS numbers: 98.80.-k; 98.80.Es

## I. INTRODUCTION

Several authors have used the SZ effect, X-rays and SGL data from galaxies and GC to provide independent estimations of cosmological parameters. The combination of X-rays and the SZ data lead to two useful cosmological tests namely, angular diameter distance  $d_A$  [1] and gas mass fraction  $f_{gas}$  of the GC [2]. Both tests have been used in the literature to investigate DE [3] and modified gravity ([4] and reference therein). Additionally, the SGL observations also can be used to probe the dark matter (DM) and DE properties [3]. Therefore, to use the GC measures constitutes an independent and complementary test to probe cosmological models. Now, from the phenomenological point of view the  $\Lambda$ CDM model is the most accepted to date, which predicts that the universe consists of approximately 4% of baryonic matter, 26% of Cold Dark Matter (CDM) and about 70% is a exotic component known as DE which is the main responsible for the accelerated expansion of the Universe nowadays. In the concordance model ( $\Lambda$ CDM) is assumed that CDM is made up of colisionless non baryonic particles and DE is driven by cosmological constant  $\Lambda$ , which has a equation of state (EoS)  $w = -1$ . From this perspective, the concordance model is in excellent agreement with the observations of Supernova Ia (SNIa), CMB anisotropies and baryonic acoustic oscillations (BAO). However,  $\Lambda$ CDM model has some unresolved fundamental issues about the nature of the of DM and DE [5, 8]. IWith respect to DE, there are different theoretical arguments against of  $\Lambda$ . The first is the coincidence problem, which establishes the question of: ¿why the value of DE and DM density have the same order of magnitud today?. Another important issue is related to “fine tuning” of the value of the cosmological constant to the present, which is in complete disagreement with quantum field theory and particle physics [6, 7]. In this way, several DE models with a dynamical EoS have been proposed to try to solve the so-called “cosmological constant problem” [7, 8].

Our main aim in this paper is to improve and update and the constraints on some well established cosmological models in the literature with the use of GC and SGL in the frame of Friedmann-Lemaître-Robertson-Walker ( $FLRW$ ) cosmology.

This paper is organized as follows. The next section (§ II) we introduce the cosmological tests and the statistical analysis. In § III we describe cosmological models of DE, including the main results. The history of expansion is analyzed in § IV. In section § V we conclude with the summary and the discussion.

---

\*Electronic address: abonilla@fisica.ufjf.br

†Electronic address: jecastillo@distrital.edu.co

## II. GALAXY CLUSTERS

### A. Angular diameter distance using SZ/X-Ray method

The thermal SZ effect is a small distortion in cosmic microwave background (CMB) spectrum due to the inverse Compton scattering of the CMB photons when they pass through the hot gas of electrons in GC [10, 11]. This small fluctuation in CMB temperature is characterized by  $\Delta T_{sz}/T_{cmb} = f(\nu, T_e)y(n_e, T_e)$ , where

$$y(n_e, T_e) = \int_{los} n_e \frac{k_B T_e}{m_e c^2} \sigma_T dl, \quad (1)$$

which is known as the Compton parameter, such that  $T_{cmb} = 2.726K$ ,  $n_e$  and  $T_e$  are the temperature of CMB, electron number density and temperature of the hot gas respectively.  $\sigma_T$  is the Thomson cross section,  $k_B$  is the Boltzmann constant,  $m_e c^2$  is the rest mass of the electron and the integration is along the line of sight (*los*). The dependence with the frequency of the thermal SZ effect is given through the term  $f(\nu, T_e)$ , which also introduces relativistic corrections (see [12] for more details and [13] for a more recent update).

On the other hand, gas in GC can reach temperatures of  $10^7 - 10^8 K$  and densities of the order of  $10^{-1} - 10^{-5} cm^{-3}$ , so they emit high amounts of energy in X-Ray. The primary emission mechanisms of X-Ray for a diffuse intra-cluster medium are collisional processes such as: free-free (Bremsstrahlung), free-bound (recombination) or bound-bound (mainly emission lines), with luminosities of the order of  $10^{44} erg/s$  or even higher and spatial extensions of several arcmin or larger, even at high redshift. X-Ray's observations currently offer a powerful technique for building catalogs of galaxy clusters, which are very important for modern cosmology [14]. The X-ray GC emission is given by

$$S_x = \frac{1}{4\pi(1+z)^4} \int n_e^2 \Lambda_{eH}(\mu_e/\mu_H) dl, \quad (2)$$

where  $\Lambda_{eH}$  is the X-ray cooling function,  $\mu$  is the molecular weight given by  $\mu_i = \rho/(n_i m_p)$  and  $z$  is the cluster redshift [1, 2]. Then, combining equations 1 and 2 through  $n_e$  we can obtain experimental cosmological distance with triaxial symmetry, given by

$$D_{c|exp}^{ell} = \frac{\Delta T_{sz0}^2}{S_{x0}} \left( \frac{m_e c^2}{k_B T_e} \right)^2 \frac{g(\beta)}{g(\beta/2)^2 \theta_{c,proj}} \frac{\Lambda_{eH}(\mu_e/\mu_H)}{4\pi^{3/2} f(\nu, T_e)^2 T_{cmb}^2 \sigma_T^2 (1+z)^4}, \quad (3)$$

where  $\Delta T_{sz0}$  and  $S_{x0}$  are the central temperature decrement and the central surface brightness respectively, which includes all the physical constants and the terms resulting from the *los* integration, such that  $\Delta T_{sz0} \propto d_A(z)$ ,  $S_{x0} \propto d_A(x)$  and  $d_A(z) = D_{c|exp}^{ell} h^{3/4} (e_{proj}/e_1 e_2)^{1/2}$ ,  $h$  is a function of GC shape and orientation,  $e_{proj}$  is axial ratio of the major to minor axes of the observed projected isophotes and  $\theta_{c,proj}$  is the projection on the plane of the sky (*pos*) (see Appendix A for some useful relationships and Table VIII for some data used in these method). The expression in Eq. 3 is a observational quantity that depends basically of the physical and geometrical properties of the cluster (see [1] for more information about the astrophysical details). That method for measuring distances is completely independent of other techniques and is valid at any redshift. We use 25 measurements of angular diameter distances from GC obtained through SZ/X-Ray method by De Filippis et al. (see Fig. 5.). In our analysis, we follow the standard procedure and minimize the  $\chi^2$  function

$$\chi_{dis}^2(z_i, \Theta) = \sum_{i=1}^{25} \frac{(D_{c|exp}^{ell}(z_i) - d_A(z))^2}{\sigma_{D_c}^2}, \quad (4)$$

where  $d_A(z)$  is the angular diameter distance In a *FLRW* universe and  $\sigma_{D_c}^2$  are the errors associated with  $D_{c|exp}^{ell}(z_i)$  (see Table VIII in Appendix).

### B. The gas mass fraction $f_{gas}$

Another independent cosmological technique is to derive  $d_A$  using the gas mass fraction data from GC. In order to use  $f_{gas}$  as cosmological test we need to assume that there is a proportion between the baryonic fraction of the GC

and the global fraction of baryonic matter and DM. Moreover, it is necessary to assume that the baryonic fraction from clusters does not depend on the redshift [15]. This assumption is valid if one considers that these clusters are formed approximately by the same time.<sup>1</sup> (see [16] for more details). Thus, the gas mass fraction can be defined as,  $f_{gas} \equiv M_{gas}/M_{tot}$ , where  $M_{gas}$  is the X-rays gas mass and  $M_{tot}$  is the total gravitational mass of GC respectively. To relate  $f_{gas}$  with the parameters of a particular cosmological model we can write  $M_{gas}$  and  $M_{tot}$  in terms of  $d_A(z)$  as follows [17],

$$f_{gas}^{\Lambda CDM}(z) \equiv \frac{b}{1 + \alpha} \frac{\Omega_b}{\Omega_{0m}} \left( \frac{d_A^{\Lambda CDM}(z)}{d_A(z)} \right)^{3/2}, \quad (5)$$

where  $d_A(z)$  is the angular diameter distance for a given cosmological model and  $d_A^{\Lambda CDM}(z)$  is the angular diameter distance for a reference model, in this case, let us assume the  $\Lambda CDM$  model. Here,  $\Omega_b$  and  $\Omega_{0m}$  are the baryonic density parameter and the DM density parameter, respectively. The parameter  $b$  is the depletion factor which relates the baryonic fraction in clusters to the mean cosmic value. The constant  $\alpha$  is the ratio between optically luminous baryonic mass in galaxies (stellar mass) to the baryonic X-ray gas mass in intracluster medium, and its value is given by  $\alpha \approx 0.19\sqrt{h}$  [16]. The factor  $h$  is the normalized Hubble constant, that is,  $h = H_0/100\text{km.s}^{-1}\text{Mpc}^{-1}$ . Let us use the  $f_{gas}$  measurements from 42 GC obtained in [18]. The  $\chi^2$  is defined as

$$\chi_{f_{gas}}^2(z_i, \Theta) = \sum_{i=1}^{42} \frac{[f_{gas}^{\Lambda CDM}(z_i, \Theta) - f_{gas}(z_i, \Theta)]^2}{\sigma_{f_{gas}}^2} + \left( \frac{\Omega_b h^2 - 0.0214}{0.0020} \right)^2 + \left( \frac{h - 0.72}{0.08} \right)^2 + \left( \frac{b - 0.824}{0.089} \right)^2, \quad (6)$$

where  $f_{gas}$  is observational gas mass fraction data [18] and  $\sigma_{f_{gas}}$  are the systematic errors. In the analysis, we have considered  $b = 0.824$  [16].

### C. Gravitational lensing

The gravitational lens effect is one of the queen's tests of General Relativity. Strong gravitational lensing occurs when the light rays of a source are strongly deflected by the lens producing multiples images. The position of these images depend on the properties of the lens mass distribution [19]. Because the Einstein radii,  $\theta_E$ , also depends on a cosmological model, the SL observations can be used as an additional method to probe the nature of the DE [3, 20]. In this work, we use the method which consists in comparing the ratio  $\mathcal{D}$  of angular diameter distances between lens and source,  $d_A(z_l, z_s)$ , and between observer and lens,  $d_A(0, z_s)$ , with its observable counterpart  $\mathcal{D}^{obs}$  given by

$$\mathcal{D}(z_l, z_s) = \frac{d_A(z_l, z_s)}{d_A(0, z_s)} = \frac{\int_{z_l}^{z_s} dz'/E(z', \Theta)}{\int_0^{z_s} dz'/E(z', \Theta)}, \quad (7)$$

$$\mathcal{D}^{obs} = \frac{c^2 \theta_E}{4\pi \sigma_{SIS}^2}, \quad (8)$$

where  $\sigma_{SIS}$  is the Singular Isothermal Sphere (SIS) velocity dispersion and  $E(z, \Theta) \equiv H(z, \Theta)/H_0$ , being  $H(z, \Theta)$  the Hubble function. In order to put constraints on cosmological parameters through  $E(z, \Theta)$ , the Einstein radius  $\theta_E$  and the dispersion velocity  $\sigma_{SIS}$  (Exactly its central velocity dispersion  $\sigma_0$ ) must be obtained by astrometric and spectroscopic means respectively. In the first case, it depends on the lens modelling (either SIS, Singular Isothermal Ellipsoid (SIE) or Navarro-Frenk-White density profiles). In the second case, the velocity dispersion  $\sigma_{SIS}$  of the mass distribution and the observed stellar velocity dispersion  $\sigma_0$  need not be the same, since the halos of DM can have a

---

<sup>1</sup> Even though GC form at the same time, they can have different evolution and so different gas fraction. To preserve the constancy of the baryon fraction with redshift to mimic the relative cosmic abundance, GC have to be selected among the most massive and relaxed ones at each epoch.

greater speed of dispersion than the visible stars [21]. These effects can be taken into account through the following relationship  $\sigma_{SIS} = f_E \sigma_0$ , where the parameter  $f_E$  emulates the systematic errors in the rms due to the difference between  $\sigma_{SIS}$  and  $\sigma_0$ ; the rms error caused by assuming the SIS model, since the observed image separation does not directly correspond to  $\theta_E$  and softened SIS potentials which tend to decrease the typical image separations [22]. In the present work we assume the best-fit reported in [20] (and references therein), where  $f_E \approx 1$ , which has been properly marginalized. On the other hand, GC can also act as sources to produce strong gravitational lensing showing giant arcs around GC. This phenomenon can be used to constrain the astrophysical properties of the cluster (projected mass) and cosmology [23]. If we assume the condition of hydrostatic equilibrium <sup>2</sup> and an approximation of spherical symmetry <sup>3</sup> [24], then a theoretical surface density can be described as

$$\Sigma_{th} = \frac{3}{2G\mu m_p} \frac{k_B T_X \beta_X}{d_A(0, z_l) \theta_c}, \quad (9)$$

where  $k_B$ ,  $m_p$ ,  $\mu = 0.6$  and  $\beta_X$  are, respectively, the Boltzmann constant, the proton mass, the mean molecular weight and the slope of the  $\beta$ -model [25]. Although the hydrostatic equilibrium and isothermal hypotheses are very strong, the total mass density obtained under such assumption may lead to good estimates, even in dynamically active GC with irregular morphologies in X-Ray. Then, combining this with the critical surface mass density for lensing  $\Sigma_{obs}$  [26], We can get a Hubble constant independent ratio as

$$\mathcal{D}^{obs} = \frac{d_A(z_l, z_s)}{d_A(0, z_s)} = \frac{\mu m_p c^2}{6\pi} \frac{1}{k_B T_X \beta_X} \sqrt{\theta_t^2 + \theta_c^2}, \quad (10)$$

where the parameters  $T_X$ ,  $\beta_X$  and  $\theta_c$  can be obtained from X-Ray observational data. The position of tangential critical curve  $\theta_t = \epsilon \theta_{arc}$ , where  $\theta_{arc}$  is the observational arc position and  $\epsilon = (1/\sqrt{1.2}) \pm 0.04$  quantifies the slight difference with arc radius angle (See [27, 28] for more details about the priors and 10 galaxy clusters used as sample).

In the present work we use a sample of 80 strong lensing systems by [20], which contains 70 data points from SLACS and LSD and 10 data points from GC. Again, the fit of the theoretical models to strong lensing observations can be found by the minimization of

$$\chi_{SL}^2 = \sum_{i=1}^{80} \frac{(\mathcal{D}_i^{obs} - \mathcal{D}_i^{th})^2}{\sigma_{\mathcal{D},i}^2}, \quad (11)$$

where the sum is over the sample and  $\sigma_{\mathcal{D},i}^2$  denotes the variance of  $\mathcal{D}_i^{obs}$ .

Additionally to these data sets defined in the subsection II A, II B, and II C, let us use 580 Supernovae data (SNIa) from Union 2.1 [29], the CMB shift parameter (Planck 2013) [30, 31], as well as data from BAO (BOSS, WiggleZ, SDSS, 6dFGS) observations, adopting the three measurements of  $A(z)$  obtained from [32, 33], and using the covariance among these data given in [34]. Each  $\chi^2$  function is constructed in a way analogous to the other tests considered above (see Appendix B).

#### D. Statistic analysis

The procedure of finding a set of parameters for a given statistic is known as Maximum likelihood  $\mathcal{L}_{max}$ , that is, given a probability distribution this is maximum for the corresponding data set. The maximum likelihood estimate for the best fit parameters  $p_i^m$  is given by

$$\mathcal{L}_{max}(p_i^m) = \exp \left[ -\frac{1}{2} \chi_{min}^2(p_i^m) \right]. \quad (12)$$

If  $\mathcal{L}_{max}(p_i^m)$  has a Gaussian errors distribution, then  $\chi_{min}^2(p_i^m) = -2 \ln \mathcal{L}_{max}(p_i^m)$ , which is our case [35]. In order to find the best values of the free parameters of the model, let us consider

<sup>2</sup> The pressure gradient force of an isothermal gas with temperature  $T_X$  is balanced by the gravity in GC.

<sup>3</sup> Specifically a hydrostatic isothermal spherical symmetric  $\beta$ -model.

$$\chi_{total}^2 = \chi_{SNIa}^2 + \chi_{CMB}^2 + \chi_{BAO}^2 + \chi_{d_A}^2 + \chi_{f_{gas}}^2 + \chi_{SGL}^2. \quad (13)$$

The Fisher matrix is used in the analysis of the constraint of cosmological models for different observational test [36, 37]. It contains the Gaussian uncertainties  $\sigma_i^2$  of the different parameters  $p_i^m$ . Given the best fit  $\chi_{min}^2(p_i^m, \sigma_i^2)$  for a set of parameters  $p_i^m$  with uncertainties  $\sigma_i^2$ , the Fisher matrix is

$$F_{ij} = \frac{1}{2} \frac{\partial^2 \chi_{min}^2}{\partial p_i^m \partial p_j^m}. \quad (14)$$

for each model  $m$ . The inverse of the Fisher matrix provides an estimate of the covariance matrix through  $[C_{cov}] = [F]^{-1}$ . Its diagonal elements are the squares of the uncertainties in each parameter marginalizing over the others, while the off-diagonal terms yield the correlation coefficients between parameters. The uncertainties obtained in the propagation of errors are given by  $\sigma_i = \sqrt{Diag[C_{cov}]_{ij}}$ . Notice that the marginalized uncertainty is always greater than (or at most equal to) the non-marginalized one: marginalization cant decrease the error, and only has no effect if all other parameter are uncorrelated with it <sup>4</sup>. Previously known uncertainties on the parameters, known as priors, can be trivially added to the calculated Fisher matrix. This is manifestly the case for us: A lot of standard cosmological datasets provide priors on our previously defined cosmological parameters. The analysis with the Fisher matrix is used to evaluate the errors on the best-fit parameters.

In our results, let us consider different cosmological models. Thus, a way to quantify which model best fit the data is consider a Bayesian comparison. We adopted the Akaike and Bayesian information criterion (AIC and BIC, respectively), which allows us to compare cosmological models with different degrees of freedom, with respect to the observational evidence and the set of parameters [38]. The AIC and BIC can be calculated as

$$AIC = -2 \ln \mathcal{L}_{max} + 2d, \quad (15)$$

$$BIC = -2 \ln \mathcal{L}_{max} + d \ln N, \quad (16)$$

where  $\mathcal{L}_{max}$  is the maximum likelihood of the model under consideration ( $\mathcal{L}_{max} = \exp[-\frac{1}{2}\chi_{min}^2]$ ),  $d$  is the number of parameters and  $N$  the number of data points. The BIC imposes a strict penalty against extra parameters for any set with  $N$  data. The preferred model is that which minimizes the AIC and BIC. However, the absolute values of them are not of interest, only the relative values between the different models [39]. Therefore the “strength of evidence” can be characterized in the form  $\Delta AIC = AIC_i - AIC_{min}$ ,  $\Delta BIC = BIC_i - BIC_{min}$ , where the subindex  $i$  refers to value of  $AIC$  ( $BIC$ ) for model  $i$  and  $AIC_{min}$  ( $BIC_{min}$ ) is the minimum value of  $AIC$  ( $BIC$ ) among all the models [40]. We give the judgements for both criterion as follows: (i) If  $\Delta AIC(\Delta BIC) \leq 2$ , then the concerned model has substantial support with respect to the reference model (i.e. it has evidence to be a good cosmological model), (ii) if  $4 \leq \Delta AIC(\Delta BIC) \leq 7$  it is an indication for less support with respect to the reference model, and finally, (iii) if  $\Delta AIC(\Delta BIC) \geq 10$  then the model has no observational support. Thus, if we have a set of models of DE, first we should estimate the best fit  $\chi^2$  and then we can apply the  $AIC$  and  $BIC$  to identify which model is the preferred one by the observations. We also apply the reduced chi-square to see how well the model fit the data, Which is defined as  $\chi_{red}^2 = \chi_{min}^2/\nu$ , where  $\nu$  is the degrees of freedom usually given by  $N - d$ . Table VI shows the values of  $d$ ,  $\chi_{red}^2$ , AIC and BIC for the DE models from all cosmological tests, whose data points are: SNIa (580), CMB (3), BAO (7),  $d_A$  (25),  $f_{gas}$  (42), SGL (80). Priors used in the present analysis are standard and most conservative possible and combining GC data with independent constraints from CMB, BAO and SNIa removes the need of priors for  $\Omega_b$  and  $h$  leads to tighter constraints over  $\Omega_m$ ,  $\Omega_k$  and the parameters that characterize the DE density for different cosmological models. On the other hand, SGL offers a great opportunity to constrain DE features without prior assumptions on the fiducial cosmology.. In what follows we present our main results.

---

<sup>4</sup> For an unbiased estimator, If all the parameters are assumed to be known (in other words, if we dont marginalize over any other parameters), then the minimal expected error is  $\sigma_i = 1/\sqrt{F_{ij}}$ .

### III. DARK ENERGY MODELS AND RESULTS

In order to put constraints on DE models using GC ( $d_A, f_{gas}$ ) and SGL, we need to compute the angular diameter distance of the model and compare it with observational datas. In addition, to investigate whether a cosmological model can predict an accelerated expansion phase of the Universe, we must study the behavior of the deceleration parameter  $q(z)$ . The angular diameter distance for a FLRW universe, from a source at redshift  $z$ , is given by

$$d_A(z, \Theta) = \frac{3000h^{-1}}{(1+z)} \frac{1}{\sqrt{|\Omega_k|}} \sin \varsigma \left( \int_0^z \frac{\sqrt{|\Omega_k|}}{E(z, \Theta)} dz \right), \quad (17)$$

where  $h = H_0/100 \text{km.s}^{-1} \text{Mpc}^{-1}$  is dimensionless Hubble parameter and the function  $\sin \varsigma(x)$  is defined such that it can be  $\sinh(x)$  for  $\Omega_k > 0$ ,  $\sin(x)$  for  $\Omega_k < 0$  and  $x$  for  $\Omega_k = 0$  [41]. In the standar FLRW cosmology, the expansion rate as a function of the scale factor  $H(a)$  is given by the Friedmann equation as

$$E^2(a, \Omega_i) = \Omega_r a^{-4} + \Omega_m a^{-3} + \Omega_k a^{-2} + \Omega_X e^{3 \int_a^1 \frac{da'}{a'} (1+w(a'))}, \quad (18)$$

where  $H(a)/H_0 = E(a, \Omega_i)$ ,  $H_0$  is the curret value of the expansion rate and the scale factor is related to redshift as  $1+z = a^{-1}$ , such that  $a_0 = 1$  at present. In the equation (18)  $\Omega_i$  is dimensionless energy densities relative to critical ( $\rho_{cri} = 3H_0^2/8\pi G$ ) in the form of the  $i$ -th component of the fluid density of: radiation ( $\Omega_r$ ), matter ( $\Omega_m$ ), curvature ( $\Omega_k$ ) and DE ( $\Omega_X$ ).  $\Omega_{r0}(h) = \Omega_\gamma(h)(1 + 0.2271N_{eff})$ , where  $\Omega_\gamma(h) = 2.46910^{-5}h^{-2}$  is the density of photons and  $N_{eff} = 3.046$  is the effective number of neutrino species [42].  $\omega(a) = p(a)/\rho(a)$  is the EoS for DE, where  $p(a)$  is the fluid pressure. This EoS divide our models into two cases: when the energy density of the fluid is constant and the other the energy density of the fluid is dynamic. In all cosmological models  $\Omega_k$  is a free parameter. A vector of parameters is considered for each DE model as  $\Theta_i^{model} = \{\theta_i, \Omega_i\}$ , where  $\theta_i = \{h, \Omega_b\}$  for the analysis of the present work.

#### A. $\Lambda$ CDM

Our analysis starts with standard cosmological model, where DE density is provided by the cosmological constant  $\Lambda$ . The expansion rate within  $\Lambda$ CDM context is given by

$$E^2(z, \Theta) = \Omega_r(1+z)^4 + \Omega_m(1+z)^3 + \Omega_k(1+z)^2 + \Omega_\Lambda, \quad (19)$$

where  $\Omega_r$ ,  $\Omega_m$  and  $\Omega_\Lambda = 1 - \Omega_m - \Omega_k - \Omega_r$ , are the density parameters for radiation, matter and DE component respectively. Here, the free parameter vector is  $\Theta = \{h, \Omega_b, \Omega_m, \Omega_k\}$ . We find the best fit of parameters at  $1\sigma$  confidence level (CL), whose results are shown in Table I.

Parameter	CMB+BAO+SNIa	CMB+BAO+SNIa+ $d_A$ + $f_{gas}$ +SGL
h	$0.6858 \pm 0.0095$	$0.7063 \pm 0.0067$
$\Omega_m$	$0.2981 \pm 0.0093$	$0.2839 \pm 0.0046$
$\Omega_k$	$-0.0011 \pm 0.0031$	$0.0048 \pm 0.0024$
$\Omega_b$	$0.0475 \pm 0.0014$	$0.04411 \pm 0.00099$
$\chi_{min}^2$	565.686	777.256

TABLE I: Summary of the best fit values for  $\Lambda$ CDM model.

In Table I we can see the impact of adding the GC and SGL tests to the more traditional ones (CMB+BAO+SNIa), which evidently improves the constraints on the parameters of the model (see Fig 1).

#### B. $w$ CDM model

The most simple extension of the  $\Lambda$ CDM model is to consider that the EoS remains constant but its value can be  $w \neq -1$ . In this case, the expansion rate for FLRW cosmology reads as

$$E^2(z, \Theta) = \Omega_r(1+z)^4 + \Omega_m(1+z)^3 + \Omega_k(1+z)^2 + \Omega_X(1+z)^{3(1+w)}, \quad (20)$$

where  $\Omega_X = (1 - \Omega_m - \Omega_k - \Omega_r)$ . In this model, the set of free parameters is  $\Theta = \{h, \Omega_b, \Omega_k, \Omega_m, \omega\}$ . As in the case of  $\Lambda$ CDM model, first we estimate the best fit values using the data from  $SNIa + CMB + BAO$  and then, we use the full data set  $SNIa + CMB + BAO + d_A + f_{gas} + SGL$ . The best fit values at  $1\sigma$  CL for this case is shown in the Table II.

Parameter	<i>CMB+BAO+SNIa</i>	<i>CMB+BAO+SNIa+d<sub>A</sub>+f<sub>gas</sub>+SGL</i>
<i>h</i>	$0.6897 \pm 0.0098$	$0.7080 \pm 0.0070$
$\Omega_m$	$0.2964 \pm 0.0093$	$0.2839 \pm 0.0049$
$\Omega_k$	$-0.0028 \pm 0.0033$	$0.0007 \pm 0.0028$
$\omega$	$-1.057 \pm 0.041$	$-1.086 \pm 0.038$
$\Omega_b$	$0.0468 \pm 0.0014$	$0.0437 \pm 0.0010$
$\chi^2_{min}$	563.953	772.283

TABLE II: Summary of the best fit values for wCDM model

Notice that in both cases the EoS has a phantom behavior and the standard model is excluded at least  $2\sigma$  CL (see Fig 1). As the case of  $\Lambda$ CDM model, the curvature parameter changes from negative to positive (Table II).

### C. Chevalier-Polarski-Linder model

Another simple extension to the  $\Lambda$ CDM model is to allow that the EoS of the DE vary with the redshift. Several parameterizations have been considered in the literature. Here, let us consider the popular Chevallier-Polarski-Linder (CPL) model [43] [44]

$$w(z) = w_0 + w_1 \frac{z}{1+z}, \quad (21)$$

where  $w_0$  and  $w_1$  are constants and the parameter  $w_1$  evaluates the dynamic character of DE. The FLRW  $E(z)$  for CPL parametrization is given by

$$E^2(z) = \Omega_r(1+z)^4 + \Omega_k(1+z)^2 + \Omega_m(1+z)^3 + \Omega_X X(z), \quad (22)$$

where  $\Omega_X = (1 - \Omega_k - \Omega_m - \Omega_r)$  and

$$X(z) = (1+z)^{3(1+w_0+w_1)} \exp \left[ -\frac{3w_1 z}{1+z} \right]. \quad (23)$$

The free parameters are  $\Theta = \{h, \Omega_b, \Omega_k, \Omega_m, w_0, w_1\}$ . The best fit values at  $1\sigma$  CL using  $CMB + BAO + SNIa$  and full data set are summarized in Table III.

We can see that CPL model in both cases the EoS ( $w_0$ ) has a quintessential behavior at present. The curvature parameter  $\Omega_k$  remains negative. The standard model remains within the  $1\sigma$  and  $2\sigma$  of CL for the present analysis (see Fig 1).

### D. Interacting Dark Energy model

Cosmological models where DM and DE are non minimally coupled throughout the evolution history of the universe, have been considered to solve the problem of the cosmic coincidence as well as the problem of the cosmological constant (models where DM interacts with vacuum energy - See [45, 46] for general review). It has recently been shown that

<i>Parameter</i>	<i>CMB+BAO+SNIa</i>	<i>CMB+BAO+SNIa+d<sub>A</sub>+f<sub>g<sub>ass</sub></sub>+SGL</i>
<i>h</i>	0.688 ± 0.011	0.7073 ± 0.0075
<i>Ω<sub>m</sub></i>	0.297 ± 0.010	0.2856 ± 0.0059
<i>Ω<sub>k</sub></i>	−0.0054 ± 0.0055	−0.0017 ± 0.0040
<i>ω<sub>0</sub></i>	−0.97 ± 0.19	−0.97 ± 0.15
<i>ω<sub>1</sub></i>	−0.50 ± 1.13	−0.71 ± 0.95
<i>Ω<sub>b</sub></i>	0.0470 ± 0.0015	0.0439 ± 0.0011
<i>χ<sub>min</sub><sup>2</sup></i>	563.854	771.481

TABLE III: Summary of the best fit values for CPL model

the current observational data can favor the late-time interaction in the dark sector [47–52]. In general, we assume that DM and DE interact via a coupling function  $Q$  given by

$$\begin{aligned}\dot{\rho}_m + 3H\rho_m &= Q\rho_m \\ \dot{\rho}_x + 3H(1+w_x)\rho_x &= -Q\rho_m,\end{aligned}\tag{24}$$

where  $\rho_m$  and  $\rho_x$  are the DM and DE density respectively, with  $w_x$  the EoS for DE. Here  $Q = \delta H$  characterizes the strength of the interacting through the dimensionless coupling term  $\delta$ , which establishes a transfer of energy from DE to DM for  $\delta > 0$ , whereas for  $\delta < 0$  the energy transfer is opposite. This model was originally introduced in [53], then investigated in various contexts [54–56]. The expansion rate of the Universe for this model is given by

$$\begin{aligned}E^2(z, \Theta) &= \Omega_r(1+z)^4 + \Omega_k(1+z)^2 + \Omega_m\Psi(z) \\ &\quad + \Omega_X(1+z)^{3(1+w_x)},\end{aligned}\tag{25}$$

where  $\Omega_X = (1 - \Omega_m - \Omega_k - \Omega_r)$  and

$$\Psi(z) = \frac{(\delta(1+z)^{3(1+w_x)} + 3w_x(1+z)^{3-\delta})}{\delta + 3w_x}\tag{26}$$

This model is characterized by the following set of parameters  $\Theta = \{h, \Omega_b, \Omega_k, \Omega_m, w_x, \delta\}$ . We show the best fit values of these parameters in Table IV.

<i>Parameter</i>	<i>CMB+BAO+SNIa</i>	<i>CMB+BAO+SNIa+d<sub>A</sub>+f<sub>g<sub>ass</sub></sub>+SGL</i>
<i>h</i>	0.703 ± 0.015	0.7165 ± 0.0092
<i>Ω<sub>m</sub></i>	0.2963 ± 0.0092	0.2844 ± 0.0049
<i>Ω<sub>k</sub></i>	−0.0048 ± 0.0036	0.0022 ± 0.0029
<i>ω<sub>x</sub></i>	−1.059 ± 0.042	−1.074 ± 0.038
<i>δ</i>	−0.0048 ± 0.0049	−0.0041 ± 0.0036
<i>Ω<sub>b</sub></i>	0.0451 ± 0.0019	0.0428 ± 0.0011
<i>χ<sub>min</sub><sup>2</sup></i>	563.960	771.442

TABLE IV: Summary of the best fit values from for IDE model.

Is interesting to note that in both cases EoS has a phantom behavior at present and the standard model is practically discarded at  $1\sigma$  CL. The curvature parameter  $\Omega_k$  is positive. We can also notice that the case  $\delta = 0$  (absence of interaction) is excluded at least to  $2\sigma$  CL for the present analysis, where we can appreciate that for both data sets the transfer of energy is from DM to DE (see Fig 1).

### E. Early Dark Energy model

In early dark energy (EDE) scenarios the DE density can be significant at high redshifts. This may be so if DE fluid tracks the dynamics of the background fluid density [57]. Here, we present the EDE model proposed by [58]. The FLRW equation for this model is



$$E^2(z, \Theta) = \frac{\Omega_r(1+z)^4 + \Omega_m(1+z)^3 + \Omega_k(1+z)^2}{1 - \Omega_X}, \quad (27)$$

where  $\Omega_X$  is given by

$$\Omega_X = \frac{\Omega_{X_0} - \Omega_e [1 - (1+z)^{3w_0}]}{\Omega_{X_0} + f(z)} + \Omega_e [1 - (1+z)^{3w_0}] \quad (28)$$

and

$$f(z) = \Omega_m(1+z)^{-3w_0} + \Omega_r(1+z)^{-3w_0+1} + \Omega_k(1+z)^{-3w_0-1}, \quad (29)$$

such that  $\Omega_{X_0} = 1 - \Omega_m - \Omega_k - \Omega_r$  is the current DE density,  $\Omega_e$  is the asymptotic early DE density and  $w_0$  is the present DE EoS. Here, we have six free parameters  $\Theta = \{h, \Omega_b, \Omega_k, \Omega_m, \Omega_e, \omega_0\}$ . The best fit values of the model parameters are summarized in Table V.

Parameter	CMB+BAO+SNIa	CMB+BAO+SNIa+ $d_A$ + $f_{gass}$ +SGL
$h$	$0.723 \pm 0.019$	$0.7154 \pm 0.0099$
$\Omega_m$	$0.295 \pm 0.010$	$0.2839 \pm 0.0050$
$\Omega_k$	$0.0072 \pm 0.0068$	$0.0032 \pm 0.0035$
$\Omega_e$	$0.043 \pm 0.029$	$0.012 \pm 0.016$
$\omega_0$	$-1.113 \pm 0.061$	$-1.087 \pm 0.040$
$\Omega_b$	$0.0425 \pm 0.0023$	$0.0429 \pm 0.0012$
$\chi^2_{min}$	564.275	771.697

TABLE V: Summary of the best fit values for EDE model.

For this model the EoS keeps its a phantom behavior at the present time and the standard model is discarded at least to  $2\sigma$  CL (see Fig 1).  $\Omega_k$  is positive in both cases.

## F. Statistical discrimination models

In Table VI we present the values for the analysis of the information criterion with respect to the five cosmological models presented above, for used data set, namely CMB+BAO+SNIa+ $d_A$ + $f_{gass}$ +SGL. As we can see,  $\Delta AIC$  and  $\Delta BIC$  are in favor of  $\omega CDM$  and  $\Lambda CDM$  respectively (approximately or less than two) and hence these models are in very good agreement with observations, which is also true for CPL, IDE and EDE models only with respect to  $\Delta AIC$ . For models CPL, IDE and EDE the value of  $\Delta BIC$  is approximately equal to seven and therefore, according to this criterion, present less observational support.

Model	$d$	$\chi^2_{red}$	AIC	$\Delta AIC$	BIC	$\Delta BIC$
$\Lambda CDM$	4	1.060	785.256	2.973	803.666	0.000
$\omega CDM$	5	1.055	782.283	0.000	805.295	1.626
CPL	6	1.055	783.481	1.198	811.096	7.430
IDE	6	1.055	783.442	1.159	811.057	7.391
EDE	6	1.055	783.697	1.414	811.312	7.646

TABLE VI: AIC and BIC analyses for different DE models using the combined analysis data sets (CMB+BAO+SNIa+ $d_A$ + $f_{gass}$ +SGL), where  $N=737$  and  $\chi^2_{red} = \chi^2_{min}/\nu$ .

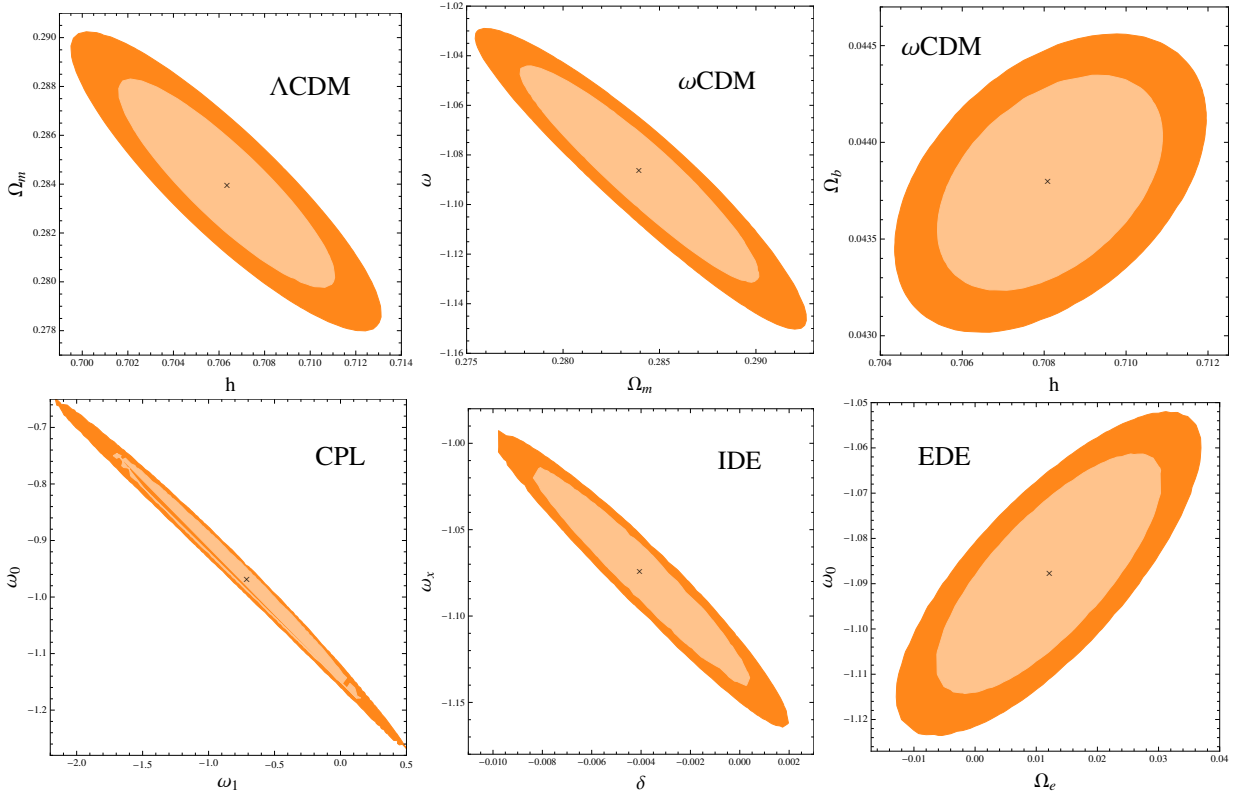


FIG. 1:  $1\sigma$  and  $2\sigma$  two-dimensional CL contours of DE cosmological models discussed, where the main results of the analysis are shown using the combined data sets (CMB+BAO+SN Ia+ $d_A$ + $f_{gas}$ +SGL).

#### IV. HISTORY OF THE EXPANSION AND COSMOGRAPHY

The kinematics of the universe can be described through the Hubble parameter  $H(t)$  and its dependence on time, i.e. the deceleration parameter  $q(t)$  [59]. Following [60], the scale factor  $a(t)$  can be expanded in Taylor series around the current time ( $t_0$ ) as:

$$\frac{a(t)}{a(t_0)} = 1 + \frac{H_0}{1!} [t - t_0] - \frac{q_0}{2!} H_0^2 [t - t_0]^2 + \frac{j_0}{3!} H_0^3 [t - t_0]^3 + \dots, \quad (30)$$

where in general we can have a kinematic description of the cosmic expansion through the set of parameters:

$$H(t) \equiv \frac{1}{a} \frac{da}{dt}; q(t) \equiv -\frac{1}{a} \frac{d^2a}{dt^2} H(t)^{-2}; j(t) \equiv \frac{1}{a} \frac{d^3a}{dt^3} H(t)^{-3}, \quad (31)$$

where the last term is known as jerk parameter  $j(t)$ . The great advantage of this method is that we can investigate the cosmic acceleration without assuming any modification of gravity theory or DE model, due mainly to its geometric approximation. Although more terms of the series can be analyzed, we are only interested in the first three terms for the present work. The deceleration and jerk parameter are obtained as

$$q(z) = -1 + \frac{(1+z)}{H(z)} \frac{dH(z)}{dz} \quad (32)$$

and

$$j(z) = q^2 + \frac{(1+z)^2}{H(z)} \frac{d^2H(z)}{dz^2}. \quad (33)$$

The history of expansion is fit through deceleration parameter, which characterize whether the universe is currently accelerated or decelerated

$$q(z) \equiv -\frac{\ddot{a}(z)}{a(z)H(z)^2}. \quad (34)$$

If  $q(z) > 0$ ,  $\ddot{a}(z) < 0$ , then the expansion decelerate as expected due to gravity produced by DM, baryonic matter or radiation. The discovery that the universe today presented an accelerated expansion already has about one decade and a half old [61] [62]. A simple explanation for this phenomenon is the cosmological constant  $\Lambda$ , which however, does not offer a consistent theoretical explanation based on physical foreground. The information about the dynamics of the expansion can be obtained through (32) and (33), which directly depends on the cosmological model. In general, if  $\Omega_X \neq 0$  is sufficiently large (i.e.  $\Omega_X > \Omega_m$ ), then  $q(z) < 0$  and  $\ddot{a}(z) > 0$ , which translates into an accelerated expansion as shown by observational. If the accelerated expansion is driven by a new type of fluid, then is important to identify if fluid energy density is constant or dynamic.

Model	$\chi^2_{red}$	Parameters
$\Lambda$ CDM	1.11	$h = 0.722 \pm 0.012$ , $\Omega_m = 0.2640 \pm 0.0093$ , $\Omega_k = -0.13 \pm 0.16$ , $\Omega_b = 0.0410 \pm 0.0014$
$\omega$ CDM	1.11	$h = 0.722 \pm 0.012$ , $\Omega_m = 0.2685 \pm 0.0093$ , $\Omega_k = -0.14 \pm 0.88$ , $\omega = -0.99 \pm 0.73$ , $\Omega_b = 0.0409 \pm 0.0015$
CPL	1.14	$h = 0.721 \pm 0.011$ , $\Omega_m = 0.274 \pm 0.013$ , $\Omega_k = -0.5 \pm 1.8$ , $\omega_a = -1.5 \pm 2.2$ , $\omega_0 = -0.60 \pm 0.50$ , $\Omega_b = 0.0411 \pm 0.0014$
IDE	1.14	$h = 0.721 \pm 0.011$ , $\Omega_m = 0.274 \pm 0.012$ , $\Omega_k = 0.2 \pm 2.5$ , $\omega_x = -1.1 \pm 3.1$ , $\delta = 3.9 \pm 13.0$ , $\Omega_b = 0.0411 \pm 0.0015$
EDE	1.14	$h = 0.720 \pm 0.012$ , $\Omega_m = 0.276 \pm 0.014$ , $\Omega_k = 0.3 \pm 1.7$ , $\omega_0 = -0.8 \pm 1.7$ , $\Omega_e = -1.1 \pm 1.7$ , $\Omega_b = 0.0412 \pm 0.0015$

TABLE VII: The best fit values for the free parameters using data from GC ( $d_A + f_{gas}$ ).

In the present cosmographic analysis we use of data from GC ( $d_A + f_{gas}$ ), where we can see that these does not provide a tight constraints on curvature and DE parameters, mainly due to the degeneracy presented between these parameters and the large systematic errors of the samples (See Table VII), which can lead to large discrepancies with respect to the standard model. Despite this, we are more interested in the analysis of the behavior of low redshift of each cosmological model with respect to these data set. Figure 2 shows the plot of the deceleration parameter  $q(z)$  and as expected, the models studied give  $q(z) < 0$  at late times and  $q(z) > 0$  at earlier epoch. All cosmological models presents a redshift of transition ( $z_t$ ) between the two periods, however, all models of dynamical DE present an interesting behavior of slowing down of acceleration at low redshift (late times), which can be characterized through the change of sign of the parameter  $j(z)$  (CPL:  $j(z_{low}) \rightarrow 0$ , when  $z_{low} \sim 0.50$ ; IDE:  $j(z_{low}) \rightarrow 0$ , when  $z_{low} \sim 0.41$ ; EDE:  $j(z_{low}) \rightarrow 0$ , when  $z_{low} \sim 0.23$ ). We can interpret  $j(z)$  as the slope at each point of  $q(z)$ , which indicates a change in acceleration. This result is consistent with the one presented by J. Barrow, R. Bean and J. Magueijo [63], who raises the possibility of a scenario consistent with the current accelerating universe and does not involve an eternal accelerated expansion. In [60] an extensive analysis of this possibility is made. This can be also a clear behavior of dynamical DE at low redshift for these models with variation of the density of DE over time.

## V. SUMMARY AND DISCUSSION

In the present work we compared alternative cosmological models of DE using data obtained from GC and SGL in addition to more traditional ones, getting the best-fit value of parameters for each one. On the other hand, applying the Akaike an Bayesian information criteria we determine which of these models is the most favored by current observational data. Our analysis shows that  $\omega$ CDM and  $\Lambda$ CDM DE models are preferred by  $\Delta AIC$  and  $\Delta BIC$ , respectively. For the first time we report that the  $\omega$ CDM model is favored by observational data at least with  $\Delta AIC$ , however, the  $\Lambda$ CDM model remains the best fit for  $\Delta BIC$ . In Figure 1 we can see that  $\Lambda$ CDM model is excluded at least  $2\sigma$  CL for  $\omega$ CDM, IDE and EDE models, combining all data set (see too Tables II, IV and V). Models as CPL, IDE and EDE, although they are penalized given their large number of free parameters, they have a good fit with the observational data.

On the other hand, we carry out the study of the history of cosmic expansion through the  $H(z)$ ,  $q(z)$  and  $j(z)$  parameters with data from GC ( $d_{A,clusters} + f_{gas}$ ). We find new evidence showing anomalous behavior of the deceleration parameter  $q(z)$  in later times ( $z_{low} < 0.5$ ), suggesting that the expansion of the universe could decelerate in the near future (Figure 2), wich was pointed out in previous works with SNIa (for CPL [64, 65]),  $f_{gas}$  (for CPL and different parameterizations of  $w(z)$  [66, 67]) and BAO (for CPL, IDE and EDE [68]). Under this perspective raises

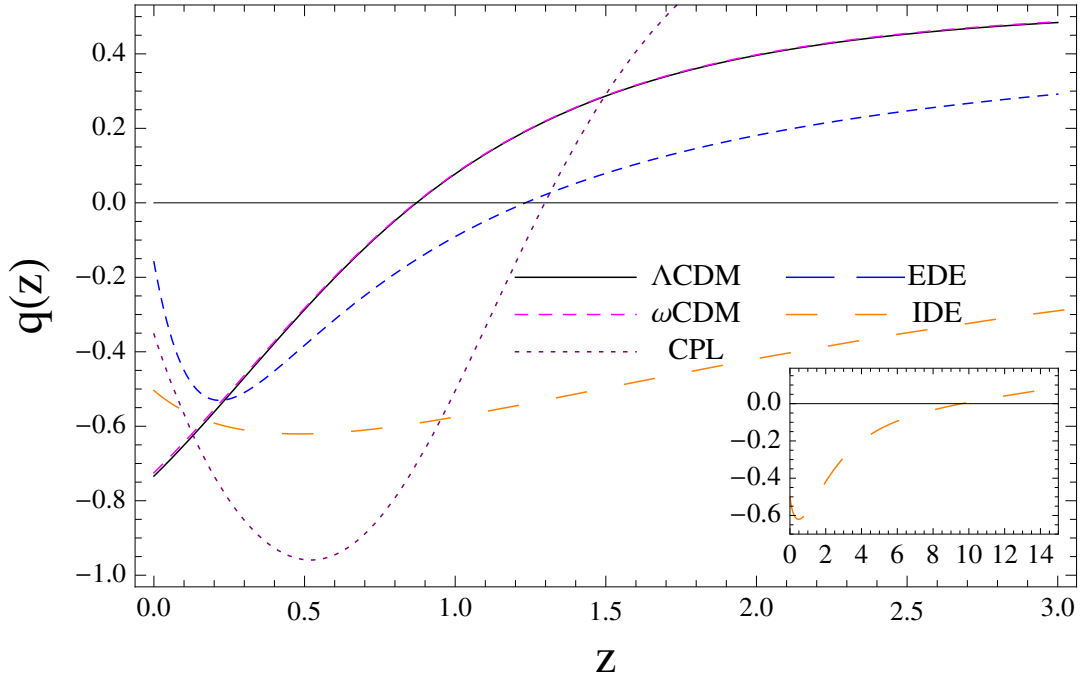


FIG. 2: Deceleration parameter vs redshift using only GC data ( $d_A + f_{gas}$ ). It is shown the transition decelerated-accelerated ( $q(z_t) = 0$ ) and the current value of ( $q_0$ ) ( $\Lambda$ CDM ( $z_t \sim 0.86$ ,  $q_0 = -0.76$ ),  $\omega$ CDM ( $z_t \sim 0.86$ ,  $q_0 = -0.76$ ), CPL ( $z_t \sim 1.32$ ,  $q_0 = -0.35$ ), IDE ( $z_t \sim 9.78$ ,  $q_0 = -0.50$ ), EDE ( $z_t \sim 1.22$ ,  $q_0 = -0.17$ )). Notice the strange behavior of the deceleration parameter to later times for models of dynamical DE (CPL, IDE, EDE).

the possibility that an accelerated expansion does not imply the eternal expansion, even in the presence of DE [60]. This cosmic slowing down of acceleration only appears in dynamic models of DE (CPL, IDE and EDE), which in principle can be an indication of the need for a scalar field such as quintessence or phantom. Finally in Figure 3 we show the results for jerk parameter  $j(z)$  obtained from our kinematic analysis, where we can appreciate a considerable deviation from  $\Lambda$ CDM (black curve) in late times ( $z < 0.5$ ) for CPL, IDE and EDE models. A more careful study might give insight into this anomalous behavior, which may also represent a challenge for alternative models to DE including modified gravity models.

As we can see, the fit of observational data acquires slightly larger values of  $\chi^2_{min}$  with respect to  $\Lambda$ CDM, when GC and SGL data are added to the more traditional ones as CMB+BAO+SN Ia, which may be mainly due to their large systematic errors (GC+SGL) (See Tables I - V). However, the potential of these data sets as cosmological tests is very high since, for example, the increase in the number of data points and the reduction of systematic errors leads to better constraints in parameters such as DE, which is fundamental interest for the cosmology.

### Acknowledgments

A. Bonilla and J. E. Castillo wish to acknowledge to the Universidad Distrital F.J.C. and FIZMAKO group for his academic support. A. Bonilla also wish to thank the Departamento de Física of the UFJF for his academic support and to Rafael Nunes for constructive and fruitful discussions.

- 
- [1] De Filippis, E., Sereno, M., Bautz, M. W. and Longo, G., *Measuring the Three-dimensional Structure of Galaxy Clusters. I. Application to a Sample of 25 Clusters*, 2005, *ApJ* 625, 108, [arXiv:astro-ph/0502153].
  - [2] Bonamente, M., Joy, M. K., LaRoque, S.J., Carlstrom, J. E., Reese, E. D. & Dawson, K.S., *Determination of the Cosmic Distance Scale from Sunyaev-Zel'dovich Effect and Chandra X-Ray Measurements of High-redshift Galaxy Clusters*, 2006, *Astrophys. J.* 647 25, [arXiv:astro-ph/0512349].

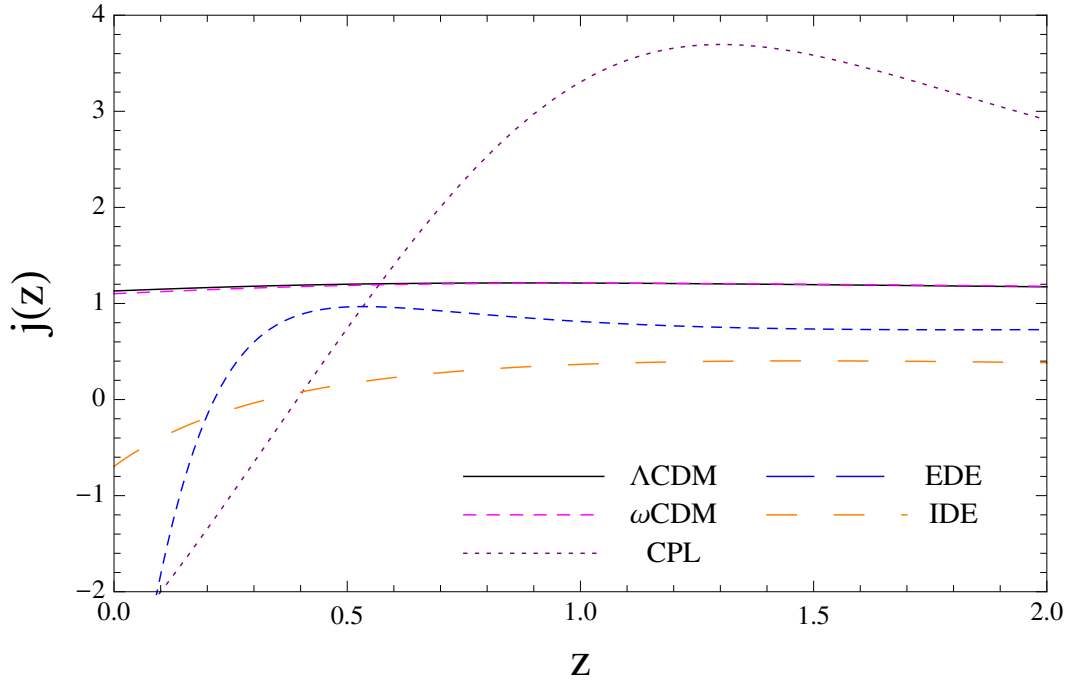


FIG. 3: Jerk parameter vs redshift using only GC data ( $d_A + f_{gas}$ ). For cosmological models CPL, IDE and EDE, we can observe a strong deviation from  $\Lambda$ CDM at present, while for  $w$ CDM this does not happen.

- [3] Biesiada, M.; Piórkowska, A.; Malec, B., *Cosmic equation of state from strong gravitational lensing systems*, 2010, Mon. Non. Roy. Astron. Soc., 406, 1055, [arXiv:astro-ph/0512349].
- [4] Campigotto, M. C., Diaferio, A., Hernandez, X., & Fatibene, L. *Strong gravitational lensing in  $f(\chi) = \chi^{3/2}$  gravity*, 2016, [arXiv:1612.01535].
- [5] Albrecht, A., Bernstein, G., Cahn, R., et al. *Report of the Dark Energy Task Force*, 2006, [arXiv:astro-ph/0609591].
- [6] Copeland, E. J., Sami, M., & Tsujikawa, S., *Dynamics of dark energy*, 2006, IJMP D 15, 1753, [arXiv:hep-th/0603057].
- [7] Weinberg, S., *The cosmological constant problem*, 1989, Rev. Mod. Phys. 61, 1.
- [8] Frieman, J. A., Turner, M. S., & Huterer, D. *Dark Energy and the Accelerating Universe*, 2008, ARA&A, 46, 385, [arXiv:0803.0982].
- [9] Bartelmann, M.; Steinmetz, M.; Weiss, A., *Arc statistics with realistic cluster potentials. 2: Influence of cluster asymmetry and substructure*, 1995, A&A 297, 1, [arXiv:astro-ph/9408082].
- [10] Sunyaev RA, Zel'dovich YB., *The Spectrum of Primordial Radiation, its Distortions and their Significance*, 1970, CoASP, 2:66–74.
- [11] Sunyaev, R. A. and Zel'dovich, Ia. B., *Microwave background radiation as a probe of the contemporary structure and history of the universe*, 1980, ARAA, 18, 537.
- [12] Itoh, N., Kohyama, Y., & Nozawa, S. *Relativistic Corrections to the Sunyaev-Zeldovich Effect for Clusters of Galaxies* 1998, ApJ, 502, 7, [arXiv:astro-ph/9712289].
- [13] Nozawa, S., Itoh, N., Suda, Y., & Ohhata, Y. 2006, Nuovo Cimento B Serie, 121, 487, [arXiv:astro-ph/0507466].
- [14] Vikhlinin, A., Kravtsov, A. V., Burenin, R. A., et al. *Chandra Cluster Cosmology Project III: Cosmological Parameter Constraints*, 2009, ApJ, 692, 1060, [arXiv:0812.2720].
- [15] S. Sasaki, *A New method to estimate cosmological parameters using baryon fraction of clusters of galaxies*, Submitted to: Publ.Astron.Soc.Jap. [arXiv:astro-ph/9611033].
- [16] S. W. Allen, R. W. Schmidt, H. Ebeling, A. C. Fabian and L. van Speybroeck, *Constraints on dark energy from Chandra observations of the largest relaxed galaxy clusters*, 2004, Mon. Non. Roy. Astron. Soc. 353, 457, [arXiv:astro-ph/0405340].
- [17] S. Nesseris and L. Perivolaropoulos, *Crossing the Phantom Divide: Theoretical Implications and Observational Status*, 2007, JCAP 0701, 018, [arXiv:astro-ph/0610092].
- [18] S. W. Allen, D. A. Rapetti, R. W. Schmidt, H. Ebeling, G. Morris and A. C. Fabian, *Improved constraints on dark energy from Chandra X-ray observations of the largest relaxed galaxy clusters*, 2007, Mon. Non. Roy. Astron. Soc. 383, 879 (2008), [arXiv:0706.0033].
- [19] Limousin, M.; Morandi, A.; Sereno, M.; Meneghetti, M.; Ettori, S.; Bartelmann, M.; Verdugo, T., *The Three-Dimensional Shapes of Galaxy Clusters*, 2012, [arXiv:1210.3067].
- [20] Cao, S.; Pan, Y.; Biesiada, M.; Godlowski, W.; Zhu, Z-H, *Constraints on cosmological models from strong gravitational lensing systems*, 2012, JCAP, 03, 016, [arXiv:1105.6226].

- [21] White, R. E., III, & Davis, D. S. *X-ray Properties of a Complete Sample of Elliptical Galaxies*, 1996, Bulletin of the American Astronomical Society, 28, 41.04.
- [22] Narayan, R., & Bartelmann, M., *Lectures on Gravitational Lensing*, 1996, [arXiv:astro-ph/9606001].
- [23] Sereno, M., & Longo, G., *Determining cosmological parameters from X-ray measurements of strong lensing clusters*, 2004, Mon. Non. Roy. Astron. Soc., 354, 1255, [arXiv:astro-ph/0409119].
- [24] Cavaliere, A., & Fusco-Femiano, R., *X-rays from hot plasma in clusters of galaxies*, 1976, A&A, 49, 137.
- [25] Rosati, P., Borgani, S., & Norman, C., *The Evolution of X-ray Clusters of Galaxies*, 2002, ARA&A, 40, 539, [arXiv:astro-ph/0209035].
- [26] Schneider, P., Ehlers, J., & Falco, E. E. 1992, Gravitational Lenses, XIV, 560 pp. 112 figs.. Springer-Verlag Berlin Heidelberg New York. Also Astronomy and Astrophysics Library, 112.
- [27] Ono, T., Masai, K., & Sasaki, S., *Cluster Mass Estimate Using Strong Gravitational Lenses Revisited*, 1999, PASJ, 51, 91.
- [28] Yu, H., & Zhu, Z.-H., *Combining optical and X-ray observations of galaxy clusters to constrain cosmological parameters*, 2011, Research in Astronomy and Astrophysics, 11, 776.
- [29] Suzuki, N., Rubin, D., Lidman, C., et al., *The Hubble Space Telescope Cluster Supernova Survey: V. Improving the Dark Energy Constraints Above  $z \approx 1$  and Building an Early-Type-Hosted Supernova Sample*, 2012, ApJ, 746, 85, [arXiv:1105.3470].
- [30] Ade, P.A.R. et al., *Planck 2013 results. XVI. Cosmological parameters*, 2014, A&A, 571, A16, [arXiv:1303.5076].
- [31] Wang, Y., & Wang, S., *Distance priors from Planck and dark energy constraints from current data*, 2013, Phys. Rev. D., 88, 043522, [arXiv:1304.4514].
- [32] Anderson L., Aubourg, E., Bailey, S., et al., *The clustering of galaxies in the SDSS-III Baryon Oscillation Spectroscopic Survey: Baryon Acoustic Oscillations in the Data Release 9 Spectroscopic Galaxy Sample*, 2012, Mon. Non. Roy. Astron. Soc., 427, 3435-3467, [arXiv:1203.6594].
- [33] Blake, C., Kazin, E. A., Beutler, F., et al., *The WiggleZ Dark Energy Survey: mapping the distance-redshift relation with baryon acoustic oscillations*, 2011, Mon. Non. Roy. Astron. Soc. 418, 1707, [arXiv:1108.2635].
- [34] Shi K., Huang Y. & Lu T., *A comprehensive comparison of cosmological models from latest observational data*, 2012, Mon. Non. Roy. Astron. Soc. 426, 2452, [arXiv:1207.5875].
- [35] Andrae, R., Schulze-Hartung, T., & Melchior, P., *Dos and don'ts of reduced chi-squared*, 2010, [arXiv:1012.3754].
- [36] Albrecht A., Amendola L., Bernstein G., Clowe D., Eisenstein D., Guzzo L., Hirata C. and Huterer D. et al., *Findings of the Joint Dark Energy Mission Figure of Merit Science Working Group*, 2009, [arXiv:0901.0721].
- [37] Wolz, L., Kilbinger, M., Weller, J., & Giannantonio, T., *On the validity of cosmological Fisher matrix forecasts*, 2012, J. Cosmology Astropart. Phys., 9, 009, [arXiv:1205.3984].
- [38] Schwarz, G., *Estimating the Dimension of a Model*, 1978, The Annals of Statistics, 6, 471.
- [39] Liddle A. R., *How many cosmological parameters?*, 2004, Mon. Non. Roy. Astron. Soc. 351, L49-L53, [astro-ph/0401198v3].
- [40] Burnham K. P. & Anderson D. R., *Model Selection and Multimodel Inference*, 2003, Technometrics, 45, 181.
- [41] Hogg DW., *Distance measures in cosmology*, 1999, [astro-ph/9905116].
- [42] Planck Collaboration, Ade, P. A. R., Aghanim, N., et al., *Planck 2013 results. XVI. Cosmological parameters*, 2014, A&A, 571, A16, [arXiv:1303.5076].
- [43] Chevallier M and Polarski D, *Accelerating Universes with Scaling Dark Matter*, 2001, Int. J. Mod. Phys. D 10, 213, [arXiv:gr-qc/0009008].
- [44] Linder E. V., *Mapping the Dark Energy Equation of State*, 2003, Phys. Rev. Lett., 90, 091301, [astro-ph/0311403].
- [45] Wang, B., Abdalla, E., Atrio-Barandela, F., & Pavón, D., *Dark Matter and Dark Energy Interactions: Theoretical Challenges, Cosmological Implications and Observational Signatures*, 2016, Reports on Progress in Physics, 79, 096901, [arXiv:1603.08299].
- [46] Bolotin, Y. L., Kostenko, A., Lemets, O. A., & Yerokhin, D. A., *Cosmological Evolution With Interaction Between Dark Energy And Dark Matter*, 2015, Int. J. Mod. Phys. D, 24, 1530007, [arXiv:1310.0085].
- [47] Kumar, S., & Nunes, R. C., *Probing the interaction between dark matter and dark energy in the presence of massive neutrinos*, 2016, Phys. Rev. D., 94, 123511, [arXiv:1608.02454].
- [48] Kumar, S., & Nunes, R. C., *Echo of interactions in the dark sector*, 2017, Phys. Rev. D. 96, 103511, [arXiv:1702.02143].
- [49] Nunes, R. C., Pan, S., & Saridakis, E. N., *New constraints on interacting dark energy from cosmic chronometers*, 2016, Phys. Rev. D., 94, 023508, [arXiv:1605.01712].
- [50] Richarte, M. G., & Xu, L., *Exploring a new interaction between dark matter and dark energy using the growth rate of structure*, 2015, [arXiv:1506.02518].
- [51] Sharov, G. S., Bhattacharya, S., Pan, S., Nunes, R. C., & Chakraborty, S., *A new interacting two fluid model and its consequences*, 2017, Mon. Non. Roy. Astron. Soc., 466, 3497, [arXiv:1701.00780].
- [52] Salvatelli, V., Said, N., Bruni, M., Melchiorri, A., & Wands, D., *Indications of a late-time interaction in the dark sector*, 2014, Phys. Rev. Lett., 113, 181301, [arXiv:1406.7297].
- [53] Wang, P., & Meng, X.-H., *Can vacuum decay in our universe?*, 2005, Classical and Quantum Gravity, 22, 283, [arXiv:astro-ph/0408495].
- [54] Costa, F. E. M., Barboza, E. M., Jr., & Alcaniz, J. S., *Cosmology with interaction in the dark sector.*, 2009, Phys. Rev. D., 79, 127302.
- [55] Nunes, R. C., & Barboza, E. M., *Dark matter-dark energy interaction for a time-dependent equation of state*, 2014, General Relativity and Gravitation, 46, 1820, [arXiv:1404.1620].
- [56] Yang, W., Banerjee, N., & Pan, S., *Constraining a dark matter and dark energy interaction scenario with a dynamical equation of state*, 2017, [arXiv:1705.09278].
- [57] Steinhardt P. J., Wang L., Zlatev I., *Cosmological tracking solutions*, 1999, Phys. Rev. D., 59, 123504, [arXiv:astro-

- ph/9812313].
- [58] Doran & Robbers, *Early Dark Energy Cosmologies*, 2006, J. Cosmology Astropart. Phys., 6, 26, [arXiv:astro-ph/0601544].
  - [59] Sandage, A., *The Change of redshift and Apparent Luminosity of Galaxies due to the Deceleration of Selected Expanding Universes*, 1962, *ApJ*. 136:319–333.
  - [60] Bolotin, Y. L., Erokhin, D. A., & Lemets, O. A., *Expanding Universe: slowdown or speedup?*, 2012, Physics Uspekhi, 55, A02, [arXiv:1108.0203].
  - [61] Perlmutter, S., Aldering, G., Goldhaber, G., et al., *Measurements of Omega and Lambda from 42 High-Redshift Supernovae*, 1999, *ApJ*, 517, 565, [arXiv:astro-ph/9812133].
  - [62] Riess, A. G., Filippenko, A. V., Challis, P., et al., *Observational Evidence from Supernovae for an Accelerating Universe and a Cosmological Constant*, 1998, *AJ*, 116, 1009, [arXiv:astro-ph/9805201].
  - [63] Barrow, J. D., Bean, R., & Magueijo, J., *Can the Universe escape eternal acceleration?*, 2000, Mon. Non. Roy. Astron. Soc., 316, L41, [arXiv:astro-ph/0004321].
  - [64] Li, Z., Wu, P., & Yu, H., *Examining the cosmic acceleration with the latest Union2 supernova data*, 2011, Physics Letters B, 695, 1, [arXiv:1011.1982].
  - [65] Shafieloo, A., Sahni, V., & Starobinsky, A. A., *Is cosmic acceleration slowing down?*, 2009, Phys. Rev. D., 80, 101301, [arXiv:0903.5141].
  - [66] Cárdenas, V. H., Bernal, C., & Bonilla, A., *Cosmic slowing down of acceleration using  $f_{gas}$* , 2013, Mon. Non. Roy. Astron. Soc., 433, 3534, [arXiv:1306.0779].
  - [67] Magaña, J., Motta, V., Cárdenas, V. H., & Foëx, G., *Testing cosmic acceleration for  $w(z)$  parameterizations using  $f_{gas}$  measurements in galaxy clusters*, 2017, Mon. Non. Roy. Astron. Soc., 469, 47, [arXiv:1703.08521].
  - [68] Bonilla Rivera, A., & García Farieta, J., *Exploring the Dark Universe: Constraint on dynamical dark energy models from CMB, BAO and Growth Rate Measurements*, 2016, [arXiv:1605.01984].
  - [69] Hu W., Sugiyama N., *Small Scale Cosmological Perturbations: An Analytic Approach*, 1996, *ApJ* 471, 542, [arXiv:astro-ph/9510117].
  - [70] Bond J. R., Efstathiou G., Tegmark M., *Forecasting Cosmic Parameter Errors from Microwave Background Anisotropy Experiments*, 1997, Mon. Non. Roy. Astron. Soc. 291, L33, [arXiv:astro-ph/9702100].
  - [71] Eisenstein, D. J., Zehavi, I., Hogg, D. W., et al., *Detection of the Baryon Acoustic Peak in the Large-Scale Correlation Function of SDSS Luminous Red Galaxies*, 2005, *ApJ*, 633, 560, [arXiv:astro-ph/0501171].
  - [72] Percival W. J. et al., *Baryon Acoustic Oscillations in the Sloan Digital Sky Survey Data Release 7 Galaxy Sample*, 2010, Mon. Non. Roy. Astron. Soc., 401, 2148, [arXiv:0907.1660].
  - [73] Eisenstein D. J., Hu W., *Baryonic Features in the Matter Transfer Function*, 1998, *ApJ*, 496, 605, [arXiv:astro-ph/9709112].
  - [74] Beutler, F., Blake, C., Colless, M., et al., *The 6dF Galaxy Survey: baryon acoustic oscillations and the local Hubble constant*, 2011, Mon. Non. Roy. Astron. Soc., 416, 30173032, [arXiv:1106.3366].
  - [75] Anderson L. et al., *The clustering of galaxies in the SDSS-III Baryon Oscillation Spectroscopic Survey: baryon acoustic oscillations in the Data Releases 10 and 11 Galaxy samples*, 2014, Mon. Non. Roy. Astron. Soc. 441, 24.

## Appendix A: Appendix A

### 1. $\beta$ -model and triaxial ellipsoids

In the distribution described by an ellipsoidal triaxial  $\beta$ -model, the electron density of the intracluster gas is assumed to be constant on a family of similar, concentric, coaxial ellipsoids. In a coordinate system relative to GC, the electron density distribution is

$$n_e = n_{e0} \left( 1 + \frac{\sum_{i=1}^3 v_i^2 x_{i,int}^2}{r_c^2} \right)^{-3\beta/2} \quad (\text{A1})$$

where  $x_{i,int}$  is the intrinsic orthogonal coordinate system centred on GC's barycenter,  $r_c$  is characteristic length scale distribution at core radius,  $v_i$  is the inverse of the corresponding core core radius,  $n_{e0}$  is the central electron density. if we take the axial ratios  $e_1 \equiv v_1/v_2$ ,  $e_2 \equiv v_2/v_3$ ,  $r_{c3} = r_c/v_3$  and and taking into account that

$$\frac{x}{a} + \frac{y}{b} + \frac{z}{c} = r_{ellp} \quad (\text{A2})$$

such that  $x_1 = x$ ,  $x_2 = y$ ,  $x_3 = z$  and  $v_1 = a^{-1}$ ,  $v_2 = b^{-1}$ ,  $v_3 = c^{-1}$  (see Fig. 4), we can obtain

$$n_e = n_{e0} \left( 1 + \frac{e_1^2 x_{1,int}^2 + e_2^2 x_{2,int}^2 + x_{3,int}^2}{r_c^2} \right)^{-3\beta/2} \quad (\text{A3})$$

with

$$\beta = \frac{\nu m_p \sigma_v^2}{k_B T_e}. \quad (\text{A4})$$

Then the electron density distribution is described by five parameters in a ellipsoidal triaxial  $\beta$ -model:  $n_{e0}$ ,  $\beta$ ,  $e_1$ ,  $e_2$  and  $r_{c3}$ .

The projection along the  $los$  of the electron density distribution, to a generic power  $m$  in the observer coordinate system is given by

$$\int_{los} n_e^m(l) dl = n_{e0}^m \sqrt{\pi} \frac{\Gamma(3m\beta - 1/2)}{\Gamma(3m\beta/2)} \frac{d_A \theta_3}{\sqrt{h}} \left( 1 + \frac{\theta_1^2 + e_{proj}^2 \theta_2^2}{\theta_{c,proj}^2} \right)^{1/2 - 3\beta/2} \quad (\text{A5})$$

where  $d_A$  is the angular diameter distance in a  $FRW$  universe,  $\theta_i \equiv x_{i,obs}/d_A$   $e_{proj}$  is the projected angular position on the plane of the sky ( $pos$ ) of the intrinsic orthogonal coordinate system  $x_{i,obs}$  and  $h$  is a function of the GC shape and orientation:

$$h = e_1^2 \sin^2 \theta_{Eu} \sin^2 \varphi_{Eu} + e_2^2 \sin^2 \theta_{Eu} \cos^2 \varphi_{Eu} + \cos^2 \theta_{Eu}, \quad (\text{A6})$$

such that  $\theta_{Eu}$  and  $\varphi_{Eu}$  are the Euler angles in the GC coordinate system (see Fig. 4) and

$$\theta_{c,proj} \equiv \theta_{c3} \left( \frac{e_{proj}}{e_1 e_2} \right)^{1/2} h^{1/4}. \quad (\text{A7})$$

If we assume that the intracluster medium is described by an isothermal triaxial  $\beta$ -model distribution with  $m=1$  we obtain

$$\Delta T_{sz} = \Delta T_{sz0} \left( 1 + \frac{\theta_1^2 + e_{proj}^2 \theta_2^2}{\theta_{c,proj}^2} \right)^{1/2 - 3\beta/2} \quad (\text{A8})$$

where  $\Delta T_{sz0}$  is the central temperature decrement of SZ effect, which is given by

$$\Delta T_{sz0} \equiv T_{cmb} f(\nu, T_e) \frac{k_B T_e}{m_e c^2} n_{e0} \sqrt{\pi} \frac{d_A \theta_{c,proj}}{h^{4/3}} \sqrt{\frac{e_1 e_2}{e_{proj}}} g\left(\frac{\beta}{2}\right) \quad (\text{A9})$$

and

$$g(\alpha) \equiv \frac{\Gamma(3\alpha - 1/2)}{\Gamma(3\alpha)}. \quad (\text{A10})$$

$e_{proj}$  is the axial ratio of the major to minor axes of the observed projected isophotes and  $\theta_{c,proj}$  is the projection on the ( $pos$ ).

On the other hand, the X-Ray surface brightness for intracluster medium with  $m=2$ , is given by

$$S_x = S_{x0} \left( 1 + \frac{\theta_1^2 + e_{proj}^2 \theta_2^2}{\theta_{c,proj}^2} \right)^{1/2 - 3\beta/2} \quad (\text{A11})$$

where the central surface brightness  $S_{x0}$  is

$$S_{x0} \equiv \frac{\Lambda_{eH}(\mu_e/\mu_H)}{4\sqrt{\pi}(1+z)^4} n_{e0} \frac{d_A \theta_{c,proj}}{h^{4/3}} \sqrt{\frac{e_1 e_2}{e_{proj}}} g(\beta), \quad (\text{A12})$$

with  $\mu_i \equiv \rho/(n_i m_p)$  the molecular weight.



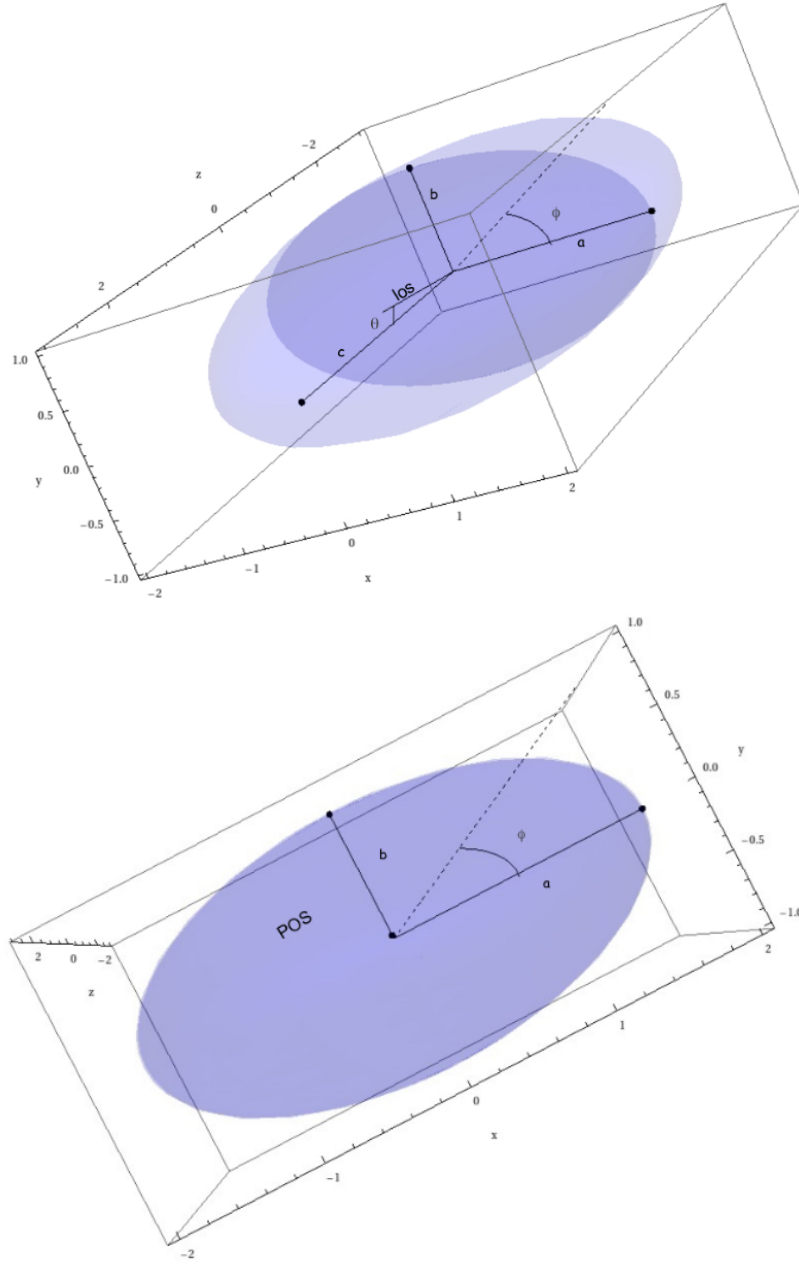


FIG. 4: Ellipsoid coefficients  $a$ ,  $b$  and  $c$ , with the  $los$  making an angle  $\theta$  with the  $z$ -axis (up). View of the  $pos$  with the  $los$  oriented along the  $z$ -axis (down).

## 2. Galaxy clusters data

Table VIII shows us the experimental cosmological distance with triaxial symmetry from De Filippis et al. obtained by the method S-Z/X-Ray [1]. Column 1 shows the cluster identification name, column 2 give the correspond redshift, column 3 is gas temperature, column 4 is central temperature decrement, column 5 is the term of dependence with frequency with relativistic corrections and column 6 show us the experimental cosmological distance. Fig 5. show us the angular diameter distance vs reshift and the data sample from De Filippis et al.

Cluster	$z_i$	$k_B T_e$ (keV)	$\Delta T_{sz0} (\mu K)$	$f(\nu, T_e)$	$D_c _{exp}^{ell}$ (Mpc)
MS 1137.5+6625	0.784	$5.7^{+1.3}_{-0.7}$	$-818^{+98}_{-113}$	2.00	$2479 \pm 1023$
MS 0451.6-0305	0.550	$10.4^{+1.0}_{-0.8}$	$-1431^{+98}_{-105}$	1.87	$1073 \pm 238$
Cl 0016+1609	0.546	$7.55^{+0.72}_{-0.58}$	$-1242 \pm 105$	1.89	$1635 \pm 391$
RXJ1347.5-1145	0.451	$9.3^{+0.7}_{-0.6}$	$-3950 \pm 350$	1.91	$1166 \pm 262$
A 370	0.374	$6.6^{+0.7}_{-0.5}$	$-785 \pm 118$	1.96	$1231 \pm 441$
MS 1358.4+6245	0.327	$7.48^{+0.50}_{-0.42}$	$-784 \pm 90$	1.88	$697 \pm 183$
A 1995	0.322	$8.59^{+0.86}_{-0.67}$	$-1023^{+83}_{-77}$	1.91	$885 \pm 207$
A 611	0.288	$6.6 \pm 0.6$	$-853^{+120}_{-140}$	1.76	$934 \pm 331$
A 697	0.282	$9.8 \pm 0.7$	$-1410^{+160}_{-180}$	1.89	$1099 \pm 308$
A 1835	0.252	$8.21^{+0.19}_{-0.17}$	$-2502^{+150}_{-175}$	1.93	$946 \pm 131$
A 2261	0.224	$8.82^{+0.37}_{-0.32}$	$-1697 \pm 200$	1.87	$1118 \pm 283$
A 773	0.216	$9.29^{+0.41}_{-0.36}$	$-1260 \pm 160$	1.76	$1465 \pm 407$
A 2163	0.202	$12.2^{+1.1}_{-0.7}$	$-1900 \pm 140$	1.90	$806 \pm 163$
A 520	0.202	$8.33^{+0.46}_{-0.40}$	$-662 \pm 95$	1.93	$387 \pm 141$
A 1689	0.183	$9.66^{+0.22}_{-0.20}$	$-1729^{+105}_{-120}$	1.86	$604 \pm 84$
A 665	0.182	$9.03^{+0.35}_{-0.31}$	$-728 \pm 150$	1.87	$451 \pm 189$
A 2218	0.171	$7.05^{+0.22}_{-0.21}$	$-731^{+125}_{-100}$	1.95	$809 \pm 263$
A 1413	0.142	$7.54^{+0.17}_{-0.16}$	$-856 \pm 110$	1.88	$478 \pm 126$
A 2142	0.091	$7.0 \pm 0.2$	$-437 \pm 25$	1.87	$335 \pm 70$
A 478	0.088	$8.0 \pm 0.2$	$-375 \pm 28$	1.91	$448 \pm 185$
A 1651	0.084	$8.4 \pm 0.7$	$-247 \pm 30$	1.75	$749 \pm 385$
A 401	0.074	$6.4 \pm 0.2$	$-338 \pm 20$	1.78	$369 \pm 62$
A 399	0.072	$9.1 \pm 0.4$	$-164 \pm 21$	1.81	$165 \pm 45$
A 2256	0.058	$9.7 \pm 0.8$	$-243 \pm 29$	1.96	$242 \pm 61$
A 1656	0.023	$6.6 \pm 0.2$	$-302 \pm 48$	1.96	$103 \pm 42$

TABLE VIII: Galaxy Cluste data set from De Filippis et al. for 25 data point (S-Z/X-Ray) [1].

## Appendix B: Appendix B

### 1. SNIa

We use the Union 2.1 compilation, which contains a sample of 580 data points. We can get the luminosity distance through the relation  $d_L(z) = (1+z)^2 d_A(z)$ , then to fit cosmological model by minimizing the  $\chi^2$  value defined by

$$\chi_{SNIa}^2 = A - \frac{B^2}{C} \quad (B1)$$

where

$$A = \sum_{i=1}^{580} \frac{[\mu_{th}(z_i, p_i) - \mu_{obs}(z_i)]^2}{\sigma_{\mu_i}^2},$$

$$B = \sum_{i=1}^{580} \frac{\mu_{th}(z_i, p_i) - \mu_{obs}(z_i)}{\sigma_{\mu_i}^2}, \quad (B2)$$

$$C = \sum_{i=1}^{580} \frac{1}{\sigma_{\mu_i}^2},$$

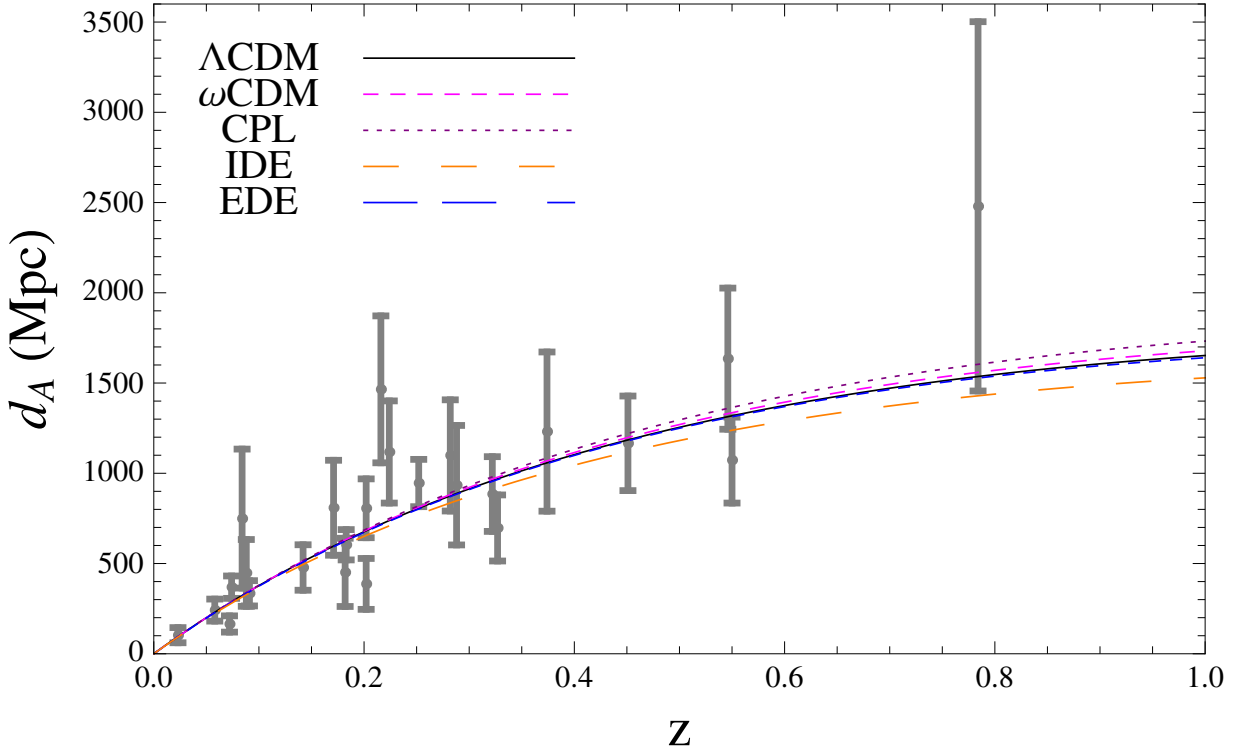


FIG. 5: Angular diameter distance vs redshift for different models with the best fit values from joint analysis (CMB+BAO+SNIa+ $d_A$ + $f_{gass}$ +SGL) and 25 data set from De Filippis et al. (Gray) [1].

where  $\mu(z) \equiv 5 \log_{10}[d_L(z)/\text{Mpc}] + 25$  is the theoretical value of the distance modulus, and we have marginalized over the nuisance parameter  $\mu_0$  and  $\mu_{obs}$ .

## 2. CMB

A standar observational test is the angular scale of sound horizon ( $r_s$ ) at time of decoupling ( $z_{cmb} \sim 1090$ ), which is encoded in the location of the first peak of the CMB power spectrum  $l_1^{TT}$ . We include CMB information of Planck 13 data [30], whose minimization is given by

$$\chi_{CMB}^2 = X_{Planck13}^T C_{cmb}^{-1} X_{Planck13}, \quad (\text{B3})$$

such that

$$X_{Planck13} = \begin{pmatrix} l_A - 301.57 \\ R - 1.7407 \\ \omega_b - 0.02228 \end{pmatrix}, \quad (\text{B4})$$

where  $\omega_b = \Omega_b h^2$ . Here  $l_A$  is the "acoustic scale" defined as

$$l_A = \frac{\pi d_A(z_{cmb})(1 + z_{cmb})}{r_s(z_{cmb})}, \quad (\text{B5})$$

where  $d_A(z_{cmb})$  is the angular diameter distance and  $z_{cmb}$  is the redshift of decoupling given by [69],

$$z_{cmb} = 1048[1 + 0.00124(\Omega_b h^2)^{-0.738}][1 + g_1(\Omega_m h^2)^{g_2}], \quad (\text{B6})$$

$$g_1 = \frac{0.0783(\Omega_b h^2)^{-0.238}}{1 + 39.5(\Omega_b h^2)^{0.763}}, g_2 = \frac{0.560}{1 + 21.1(\Omega_b h^2)^{1.81}}, \quad (\text{B7})$$

The “shift parameter”  $R$  is defined as [70]

$$R = \frac{\sqrt{\Omega_m}}{c} d_A(z_{cmb})(1 + z_{cmb}). \quad (\text{B8})$$

$C_{cmb}^{-1}$  in Eq. (B3) is inverse covariance matrix for  $(R, l_A, \omega_b)$ , which to Planck 13 data is:

$$C_{cmb}^{-1} = \sigma_i \sigma_j C_{NorCov_{i,j}}, \quad (\text{B9})$$

where  $\sigma_i = (0.18, 0.0094, 0.00030)$  and normalized covariance matrix is:

$$C_{NorCov_{i,j}} = \begin{pmatrix} 1.0000 & 0.5250 & -0.4235 \\ 0.5250 & 1.0000 & -0.6925 \\ -0.4235 & -0.6925 & 1.0000 \end{pmatrix}. \quad (\text{B10})$$

This test contributes with 3 data points to the statistical analysis.

### 3. BAO

The large scale correlation function measured from SDSS, includes a peak which was identified with the expanding spherical wave of baryonic perturbations from acoustic oscillations at recombination, whose current comoving scale corresponds to  $150 Mpc$ . The expected BAO scale depends on the scale of the sound horizon at recombination and on transverse and radial scales at the mean redshift of galaxies in the survey. To obtain constraints on cosmological model we begin with  $\chi^2$  for WiggleZ BAO data [33], which is given by

$$\chi_{WiggleZ}^2 = (\bar{A}_{obs} - \bar{A}_{th}) C_{WiggleZ}^{-1} (\bar{A}_{obs} - \bar{A}_{th})^T, \quad (\text{B11})$$

where  $\bar{A}_{obs} = (0.447, 0.442, 0.424)$  is data vector at  $z = (0.44, 0.60, 0.73)$  and  $\bar{A}_{th}(z, p_i)$  is given by [71]

$$\bar{A}_{th} = D_V(z) \frac{\sqrt{\Omega_m H_0^2}}{cz}, \quad (\text{B12})$$

in which  $D_V(z)$  is the distance scale defined as

$$D_V(z) = \frac{1}{H_0} \left[ (1+z)^2 d_A(z)^2 \frac{cz}{E(z)} \right]^{1/3}. \quad (\text{B13})$$

Here,  $d_A(z)$  is the angular diameter distance. Additionally,  $C_{WiggleZ}^{-1}$  is the inverse covariance matrix for the WiggleZ data set given by

$$C_{WiggleZ}^{-1} = \begin{pmatrix} 1040.3 & -807.5 & 336.8 \\ -807.5 & 3720.3 & -1551.9 \\ 336.8 & -1551.9 & 2914.9 \end{pmatrix}. \quad (\text{B14})$$

Similarly, for the SDSS DR7 BAO distance measurements,  $\chi^2$  can be expressed as [72]

$$\chi_{SDSS}^2 = (\bar{d}_{obs} - \bar{d}_{th}) C_{SDSS}^{-1} (\bar{d}_{obs} - \bar{d}_{th})^T, \quad (\text{B15})$$

where  $\bar{d}_{obs} = (0.1905, 0.1097)$  is the data points at  $z = 0.2$  and  $z = 0.35$ . Here,  $\bar{d}_{th}(z_d, p_i)$  denotes the distance ratio

$$\bar{d}_{th} = \frac{r_s(z_d)}{D_V(z)}, \quad (\text{B16})$$

in which  $r_s(z)$  is the comoving sound horizon given by

$$r_s(z) = c \int_z^\infty \frac{c_s(z')}{H(z')} dz', \quad (\text{B17})$$

and  $c_s(z)$  is the sound speed

$$c_s(z) = \frac{1}{\sqrt{3(1 + \bar{R}_b/(1+z))}}, \quad (\text{B18})$$

with  $\bar{R}_b = 31500\Omega_b h^2 (T_{CMB}/2.7\text{K})^{-4}$  and  $T_{CMB} = 2.726\text{K}$ . The redshift  $z_{drag}$  at the baryon drag epoch is fitted with the formula proposed in [73],

$$z_{drag} = \frac{1291(\Omega_m h^2)^{0.251}}{1 + 0.659(\Omega_m h^2)^{0.828}} [1 + b_1(\Omega_b h^2)^{b_2}], \quad (\text{B19})$$

where

$$b_1 = 0.313(\Omega_m h^2)^{-0.419} [1 + 0.607(\Omega_m h^2)^{0.674}] \quad (\text{B20})$$

and

$$b_2 = 0.238(\Omega_m h^2)^{0.223}. \quad (\text{B21})$$

Here  $C_{SDSS}^{-1}$  is the inverse covariance matrix for the SDSS data set given by

$$C_{SDSS}^{-1} = \begin{pmatrix} 30124 & -17227 \\ -17227 & 86977 \end{pmatrix}. \quad (\text{B22})$$

For the 6dFGS BAO data [74], there is only one data point at  $z = 0.106$ , the  $\chi^2$  is easy to compute

$$\chi_{6dFGS}^2 = \left( \frac{d_z - 0.336}{0.015} \right)^2. \quad (\text{B23})$$

Additionally, we include measures from the Main Galaxy Sample of Data Release 7 of Sloan Digital Sky Survey (SDSS-MGS) [75]  $r_s/D_V(0.57) = 0.0732 \pm 0.0012$ . Then, the total  $\chi_{BAO}^2$  is given by

$$\chi_{BAO}^2 = \chi_{WiggleZ}^2 + \chi_{SDSS}^2 + \chi_{6dFGS}^2 + \chi_{SDSS-MGS}^2 \quad (\text{B24})$$